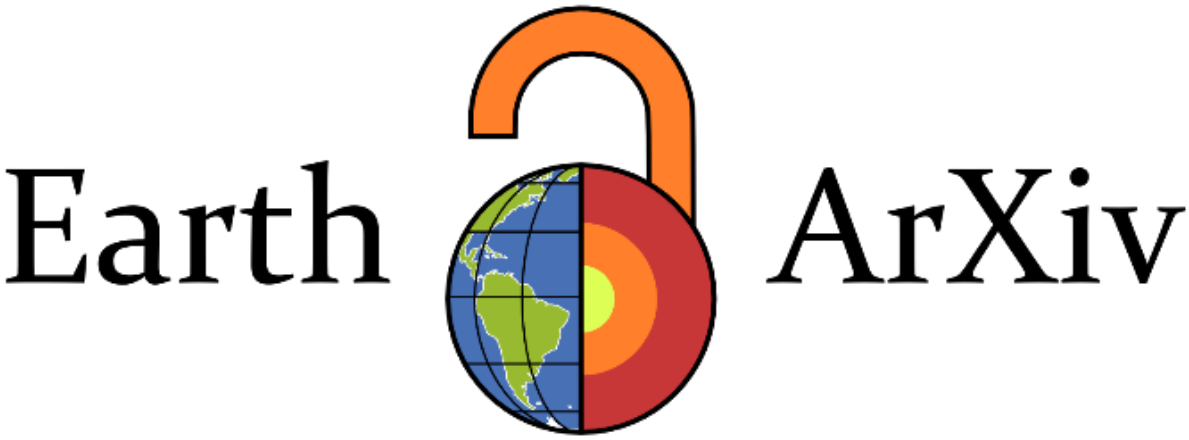

Hydrologic Implications of Seasonally Draining Lakes in the Central Oregon Cascades

A. Simpson[1], E. Levenson[2], L. Karlstrom[1], S. Cooley[2,3]

[1]University of Oregon, Department of Earth Science
[2]University of Oregon, Department of Geography
[3]Duke University, Earth and Climate Sciences

Key Points:

- Drainage of seasonal lakes constrains Holocene lava dam permeability.
- Scale dependent transmissivity implies heterogeneous aquifer.
- Seasonal lake retention times are correlated with snowpack.

Corresponding author: A. Simpson, asimps10@uoregon.edu

Abstract

The hydrogeology of volcanic terrain exhibits characteristics that reflect both a legacy of volcanic construction and transient evolution of bedrock hydraulic conductivity on million year timescales. Here, we study a drainage basin in the Central Oregon High Cascades in which Holocene lava flows dammed streams, creating seasonal lakes that fill with the spring snowmelt, and drain completely over the summer. The filling and draining of these lakes depends both on the volume of snowmelt and the permeability of their porous lava dams, providing a natural experiment for disentangling multiscale hydraulic properties from climate. We measure the drainage of two seasonal lakes in the watershed of permanent Clear Lake (the highest elevation permanent source of the McKenzie River) with in situ sensors and satellite remote sensing, and compare this with the larger scale summer recession of the McKenzie river at the outlet of Clear Lake. Clear Lake recession is modeled with 2 parallel linear reservoirs, which are linked to aquifer properties and imply watershed scale transmissivity that varies with spatial scale of the aquifer. We also find, using remote sensing-derived timeseries, that all three systems, but particularly the draining lakes, have responded to declining snowpack since 1990. These results suggest that seasonal variations in surface water storage encode the structure of volcanic aquifers generally, and can be used to infer groundwater dynamics in the Cascade Range.

Plain Language Summary

The Oregon Cascades are home to thousands of lakes, some of which are seasonal. We investigate Lost Lake and Fish Lake, lakes that are bordered by some of the youngest basaltic lava flows in the Central Oregon cascades. Unweathered basaltic lava is permeable and sucks up precipitation like a rocky sponge, where it then flows underground. Lost Lake and Fish Lake were rivers until they were dammed by the young lava flows at 2.7−7.4 ka. They get inundated with water during the spring snowmelt, and a lake forms that slowly drains over the summer. We deployed sensors on the lakebeds to measure lake levels from 2022-2024, and extend this data record back to 2017 using satellite remote sensing imagery. Permeability is estimated by modeling lake drainage into the porous substrate. We compare the drainage of these seasonal lakes to streamflow recession of nearby Clear Lake, a permanent, but also lava-dammed, lake whose basin contains the smaller seasonal systems. We find that the inferred hydrologic properties vary systematically with inferred spatial scale, indicating heterogeneity of the groundwater system. The dynamics of recession/draining in all three systems are correlated to snowpack, which has exhibited a declining trend since 1990.

1 Introduction

Landscapes constructed from young, dominantly basaltic (mafic composition) lava flows and intrusions inherit highly anisotropic and multiscale permeability associated with lava flow structures such as: cooling joints, brecciated interfaces, and lava tubes. These macro-porosity features have some similarities to karst (Ford & Williams, 2007), although their physical origin differs. For example, porosity increases through time in karst systems due to chemical weathering, but generally decreases through time in volcanic deposits as porosity is occluded due to fines infiltration (Porder et al., 2007) and chemical weathering (Lohse & Dietrich, 2005). In wet climates, the groundwater dynamics of young volcanic landscapes (flow ages less than ~ 2 Ma (Karlstrom et al., 2025)) dominate hydrographs of surface streams, as infiltration dominates runoff due to the high vertical permeability. These young landscapes are able to transmit vast quantities of water (Swarzenski et al., 2017; Brooks et al., 2025; Tague & Grant, 2004), and can host massive regional aquifers (Karlstrom et al., 2025; Lindholm, 1996). The High Cascades Province of the Central Oregon Cascades is home to one such young volcanic aquifer (Tague & Grant, 2004; Jefferson et al., 2006).

The Oregon Cascades is divided into two geologic provinces, the High Cascades and the Western Cascades (Taylor, 1990). The High Cascades are young (< 2 Ma) basalts that are highly permeable (Tague & Grant, 2004; Karlstrom et al., 2025). Streams sourced from this province have low annual variation in discharge and large summer baseflow in the absence of recharge (Tague & Grant, 2004; Karlstrom et al., 2025). The High Cascades hosts a regional aquifer that sustains summer streamflow (Tague & Grant, 2004; Karlstrom et al., 2025). The Western Cascades are older ($> 2-7$ Ma) basalts that are less permeable (Tague & Grant, 2004; Jefferson et al., 2010; Karlstrom et al., 2025). As a result, the province is highly channelized. Its streams are flashy and runoff dominated, baseflow derives from local hillslopes that drain over the summer (Tague & Grant, 2004).

Volcanic effusion rates in the High Cascades outpace erosion, leading to a > 1 km thick mass of undissected lava, volcanic edifices, and young intrusions that define the topographic crest of the mountain range and orographic precipitation gradient (O'Hara & Karlstrom, 2023). Large amounts of precipitation recharge an aquifer > 80 km^3 in volume, largely confined to younger High Cascades rocks near the summit of the range (Karlstrom et al., 2025). The adjoining Western Cascades province exhibits hydrogeologic characteristics more typical of fractured mountain bedrock landscapes (Gabrielli et al., 2012). The High Cascades aquifer sustains summer streamflow to the Willamette River to the west and Deschutes River to the east, with cold stream temperatures and steady discharge that provide critical habitat for salmon and native bull trout (Tague et al., 2007). Despite comprising 12.5% of the Willamette River's watershed area, water from this region accounts for 30% - 75% of summer streamflow near its confluence with the Columbia River (Brooks et al., 2025). However, the hydrogeologic structure of this landscape and the resilience of its groundwater resources to climate change are understudied.

Groundwater research in the High Cascades is hampered by a lack of well data and steep, forested terrain that impedes geophysical measurements. Previous studies have modeled spring discharge on the eastern side of the range (Manga, 1996, 1997), inferred groundwater flow from temperature-depth profiles in the few geothermal exploration wells (Ingebritsen et al., 1992; Karlstrom et al., 2025; Saar & Manga, 2004), and examined stable isotopes from springs (James et al., 2000; Jefferson et al., 2006). A regional groundwater flow model of the Deschutes river watershed (including the eastern slopes of the High Cascades) found that 0.9 km^3 of water crosses the crest into the east each year (Gannett et al., 2017), which suggests that topography alone does not control hydrologic pathways.

In this study, we aim to evaluate the multiscale groundwater dynamics in a single catchment of the volcanic Central Oregon Cascades. To do this, we measure the filling and draining of two seasonal lakes using pressure transducers and satellite remote sensing data. These lakes have no permanent surface outlet and drain through their permeable lakebeds in the summer. We idealize their draining as a natural falling head permeameter test to calculate the permeability and transmissivity of these lakebeds. We compare the draining of these seasonal lakes to summer baseflow recession from the outlet of a groundwater-fed permanent lake (Clear Lake), whose watershed contains the seasonal lakes. We model this streamflow recession as the drainage of 2 parallel linear reservoirs to calculate a watershed-scale transmissivity, and compare these 3 transmissivity values to other measurements in the region. Long-term satellite remote sensing data illuminates changes in the filling and draining of the seasonal lakes as regional snowpacks decline, providing some insight into expected future groundwater dynamics in a changing climate.

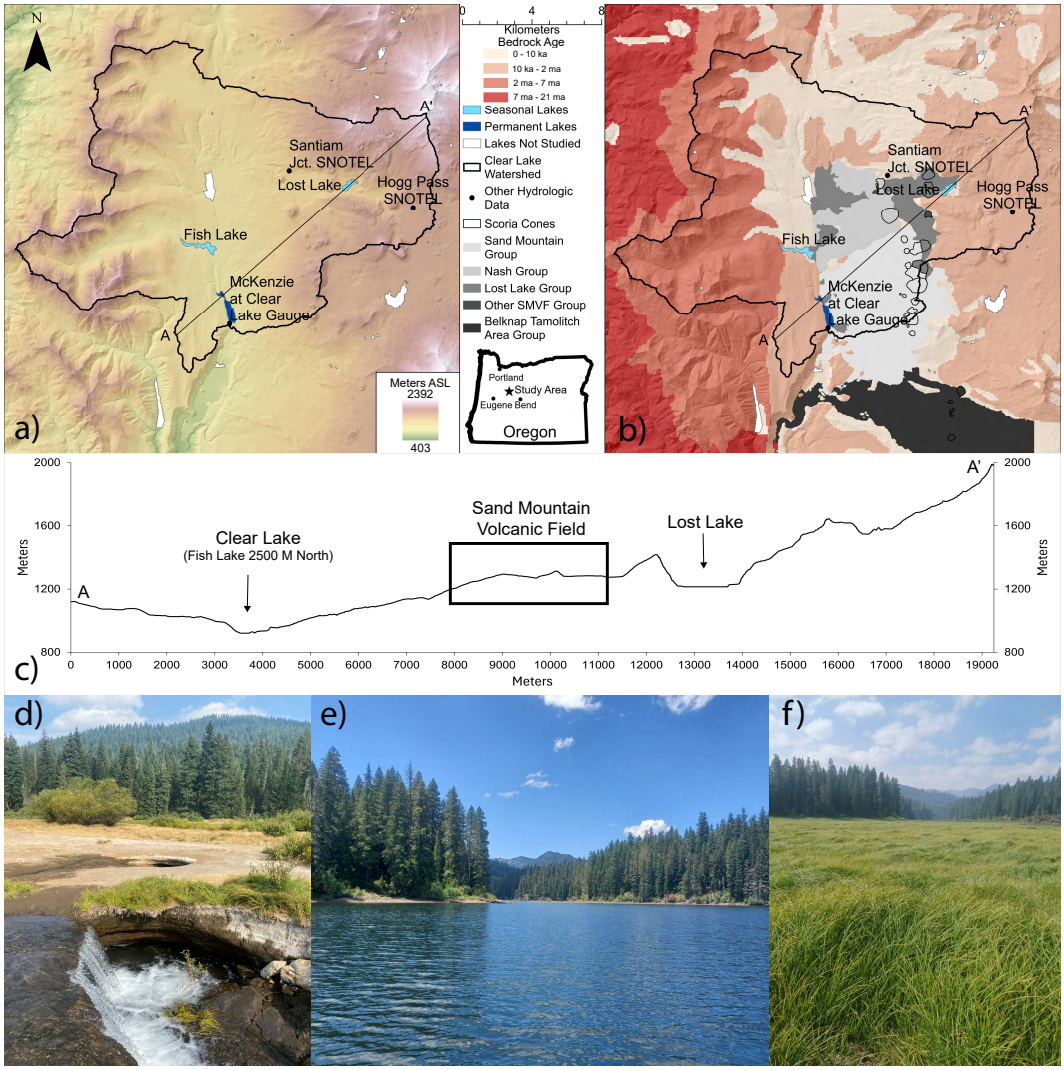

Figure 1. a) Map of study area, showing lakes as polygons. The three labeled lakes are the focus of this study. SNOTEL sites at Hogg Pass and Santiam Junction are labeled, as is the USGS streamflow gauge at the outlet of Clear Lake. b) Map of bedrock ages in study area (Sherrod & Smith, 2000), along with flows and scoria cones of the Sand Mountain Volcanic Field (Deligne et al., 2016). c) Cross section of A-A' line, with the rough location of the Sand Mountain Volcanic Field highlighted. d) Sinkholes (possibly lava tubes, partially filled with tephra from the Sand Mountain eruptions (McKay, 2012)) in the bed of Lost Lake that water flows into. e) Fish Lake in June. f) Fish Lake in August. Photos by Leif Karlstrom (d) and Alex Simpson (e-f).

2 Methods: Data

2.1 Study Site

Our study area encompasses the 238 km^2 watershed of Clear Lake (44.3684 N, -121.9949 E), the highest elevation permanent source of the McKenzie river, which flows from its outlet (Figure 1). Lost Lake (44.4323 N, -121.9067 E) and Fish Lake (44.4012 N, -122.0137 E) are two highly seasonal lakes located within the Clear Lake watershed.

Within the watershed is a series of basaltic-andesite Holocene (2.7−7.4 ka) lava flows from the Sand Mountain Complex (Deligne et al., 2016). These lava flows feature morphologies typical of basaltic lava flows, with blocky jointed interiors and rubbly flow tops/bottoms, and many were fed by lava tubes (Deligne et al., 2016). Clear Lake is bordered by these lavas on its eastern shore (Figure 1b), where numerous springs and seeps can be found underwater (Stearns, 1929). Lost Lake and Fish Lake border these lava flows "upstream" of Clear Lake (Figure 1b). All 3 lakes were formed in antecedent river valleys that were dammed by these lava flows (Taylor, 1990), and stream channels can be seen flowing in Lost Lake and Fish Lake even when the lakes have drained (Figure 2a and e). Lost Lake has no surface outlet and appears to drain down macropores (perhaps lava tubes partially filled with tephra, Figure 1d, although joint and brecciated flow tops/bottoms are also possible) in its lakebed. Similar structures have been reported at Fish Lake, although it also has an ephemeral surface outlet leading to nearby Clear Lake. Lost Lake was a High Cascade stream that was dammed by the Sand Mountain lava flows. Fish Lake was a Western Cascade stream before being dammed. 75% of Clear Lake's watershed is within the High Cascades province, and it shows characteristics of High Cascades streams. The rest of its watershed is in the Western Cascades. Clear Lake itself sits at the boundary of the High and Western Cascades. There is a graben structure at this boundary, and Clear Lake is underlain by a basin-fill diamict unit (Black et al., 1987).

2.2 Discharge and Precipitation Data

A USGS gauge (14158500) measures discharge of the McKenzie River just downstream from the outlet of Clear Lake. Daily discharge data has been collected continuously since 1947. However, we only use data from water years 1990-2024 to align with the temporal range of available remote sensing data for Lost and Fish Lakes. We use unit discharge in mm/day for our analysis (computed by dividing discharge by Clear Lake drainage area of 238 km^2), but refer to it as discharge in the rest of this study. Clear Lake's level is nearly static year round, yet it discharges 27 times its volume in an average water year. With a retention time of 14 days (Johnson et al., 1985), discharge from Clear Lake in the typically dry summers of the region reflects drainage of the regional aquifer.

There are 2 SNOTEL sites in the watershed of Clear Lake, Santiam Junction at 1140 m elevation and Hogg pass at 1463 m. Daily precipitation and snow-water equivalent (SWE) data has been collected since 1978 for Santiam Jct. and 1979 for Hogg Pass. Like discharge data from Clear Lake, only data from the 1990-2024 water years are used in this study. This region has cold, wet winters and warm, dry summers (Figure 4a). Total precipitation is the same at both stations, 2 m/year on average. Precipitation is predominantly rain, with snow a significant but declining portion. From water year 1990 to 2024, snow went from being 43% to 32% of precipitation at Hogg Pass, and 28% to 20% of precipitation at Santiam Junction. Maximum snowpack is declining at a rate of 0.4 mm/year at Santiam Junction, and 19 mm/year at Hogg Pass.

Lost Lake and Fish Lake lose water to evaporation in addition to seepage. This flux must be considered as it may artificially increase the seepage rate. Although direct measurements are not available at Lost and Fish Lakes, it is reasonable to assume similar evaporation rates as at nearby Crater Lake (another high elevation Cascade lake $\sim$ 160 km to the southwest) of 76 cm/year (Redmond, 2007). A water budget for springs east of the crest imply ET rates of 43-98 cm/year (Manga, 1997), indicating that evaporation from Crater Lake is reasonably representative of the entire region. Assuming a constant evaporation throughout the year means the lakes lose 2 mm/day. But evaporation is not constant year round, and estimates from a meteorological buoy on Crater Lake indicate late summer and early autumn (Aug-Nov) have the greatest evaporation rates (Redmond, 2007). The water-air temperature difference is at its greatest during this time, and wind speeds increase towards their winter maximums. Evaporation also occurs in the winter, at a higher rate than in late spring/early summer, even when precipitation

is falling. Thus, 2 mm/day is likely an upper bound of evaporation during lake drainage in the early summer (Jun-Jul), and a lower bound during lake drainage in the winter.

2.3 In Situ Measurements

We use a combination of remote sensing and direct instrumental measurement to quantify the rate of draining for Lost and Fish lakes. Onset Hobo Pressure-Temperature transducers are used to collect pressure-temperature data, which is converted to height of water above the sensor via hydrostatic balance (see Appendix A for more details). We note these values do not equal maximum lake depth, as the sensors were not deployed in the deepest part of the lakes (Figure 3). We obtained 1 year of water depth data for Fish Lake, the 2024 water year (Oct 1st to Sep 30th), and 2 years for Lost Lake, the 2023-2024 water years (Figure 4c).

Lake levels have a broadly similar temporal signature to discharge from Clear Lake; however, the lakes often run dry while Clear Lake experiences a long recession in the summer (Figure 4b-c). There are several smaller drainage events each year before the final drainage in the summer (distinguished from periods where the lake was full in part through measured temperature of the sensor, see Appendix A and Figure 4c). The full extent of drainage measured by our in situ sensors is not known, since the sensors were not at the deepest part of the lake. Drainage periods longer than 14 days are chosen to quantify the rate of lake drainage (Figure 4c). The start of each drainage event is peak level before the start of the decline and the end is when water level begins to increase again, or when the sensor reaches 0 in the summer.

2.4 Remote Sensing

We extend our lake drainage record back to 2017 using optical satellite imagery time series of lake area (Figure 5). Satellite-based lake area time series are generated using PlanetScope surface reflectance imagery with ~ 3 m spatial resolution and daily temporal resolution. Cloud cover reduces valid observations to a "near-daily" frequency. To estimate lake area, we first reprojected each image to UTM zone 10N. Due to the variations in atmospheric conditions and radiometric calibration between PlanetScope sensors (Houborg & McCabe, 2016), as well as differences in shoreline complexity and vegetation reflectance values among lakes, a universal water classification approach was unsuitable given the precision required for this study. In Fish Lake, the similarity in reflectance values between open water and the forested hillside prevented us from classifying open water using Normalized Difference Water Index (NDWI) (McFeeters, 1996) values. Given the relatively simple shoreline, we manually digitized lake polygons in QGIS for each image and recorded the area in km^2. An NDWI thresholding approach is more suitable for Lost Lake, where the presence of emergent vegetation produces a more complex shoreline and a bimodal NDWI histogram. Therefore, we converted PlanetScope images of Lost Lake to NDWI images, and classified water using an Otsu threshold (Otsu, 1979). We manually inspected each image and removed observations from the time series that were negatively affected by atmospheric conditions. Due to snow, ice, and cloud cover this data is only reliable in summer, when the lakes drain.

Monthly resolution ESA GSWO (Pekel et al., 2016) satellite remote sensing optical band data are too temporally coarse for model validation, but do capture long term trends in lake surface areas. We downloaded the Pacific Northwest tile for each month from April 1984 to December 2021. We use data from the 1990 water year onwards, as early Landsat data had many erroneous values (0 values in between two full values). We defined masks for all 3 lakes and added up each grid of water within the lake masks to get the mean surface area that month (Figure 2). We analyze long term trends in lake surface area, as surface area is related to depth and volume of water in the lake.

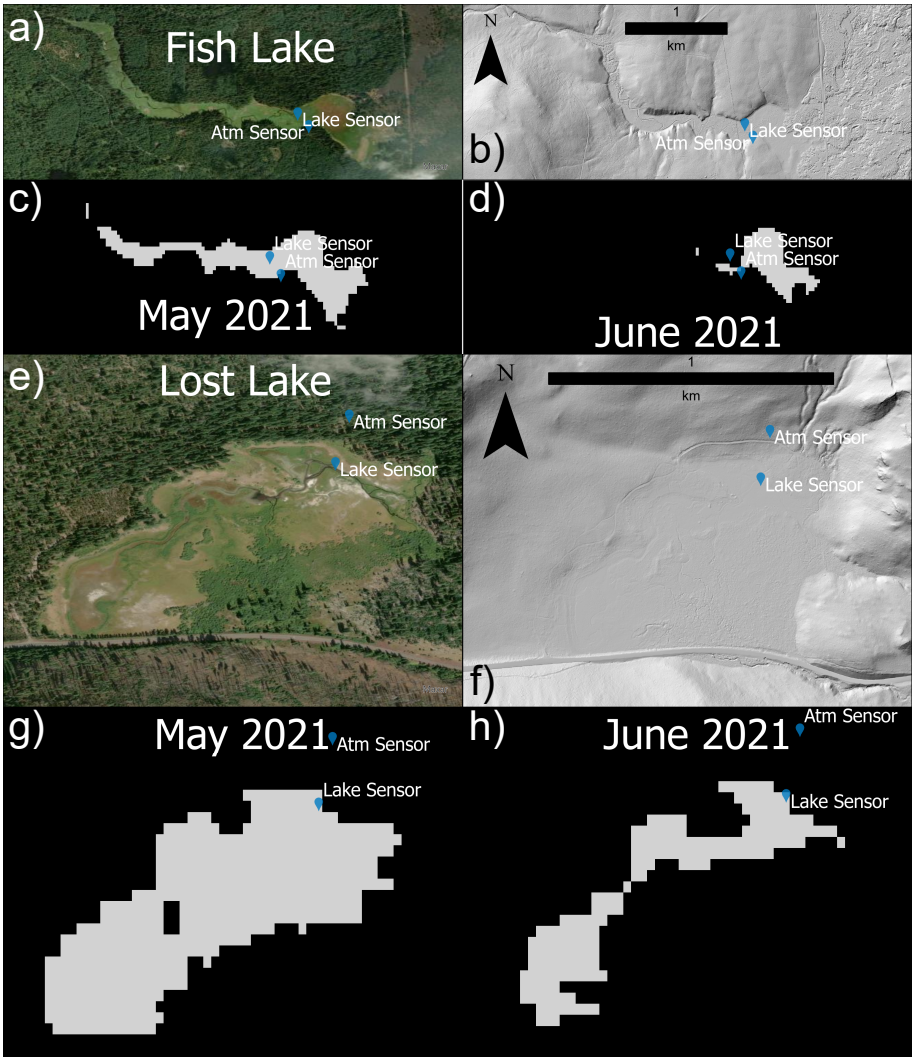

Figure 2. Workflow for processing GSWO data. **(a)** and **(e)** Satellite images; **(b** and **(f)** hillshade of 1-m LiDAR digital elevation models. **(c)-(d)** Lake surface area of Fish Lake at two times in 2021, sensor locations marked. **(g)** and **(h)** Lake surface area for Lost Lake at two times in 2021, sensor locations marked.

Using known heights from the pressure sensor and known areas from remote sensing data, we then derive hypsometries to convert satellite derived surface area data into lake depth. The Lost Lake depth-area relationship was produced with 2023 data (Figure 6a) and validated with 2024 data (Figure 6b). The average misfit of 0.12 m from Lost Lake's validation is used for all satellite data. The satellite data does not capture the maximum possible extent, based on shorelines, and the sensors do not capture the full drainage of the lakes since they are not in the lowest points of the lakes. Known lakebed geometry from Oregon Department of Geology and Mineral Industries (DOGAMI) ~ 1 m horizontal resolution LiDAR DEMs are used to fill in these blanks. These DEMs have a vertical accuracy of 3 cm. Unfortunately, the western edge of Fish Lake shows tinning artifacts. This may be because Fish Lake is at the border of two different LiDAR acquisition programs (one run by DOGAMI, the other by the US Forest Service), or there may have been water in it during that specific acquisition. We convert surface area data to

depth by interpolating along the hypsometry (Figure 3), and the sensor data is corrected for the static offset between the sensor and the bottom of the lake.

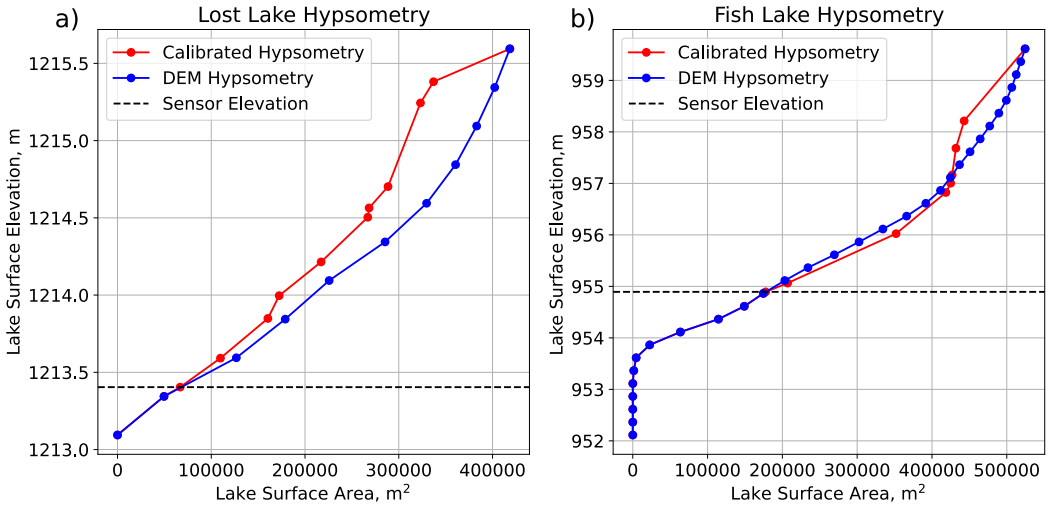

Figure 3. Hypsometries for Lost (a) and Fish (b) Lakes. The red curves are calibrated hypsometries derived from in situ sensor depth and corresponded satellite-derived surface areas, and blue curves are hypsometries derived from LiDAR DEMs of the lakebeds. The black dashed lines are the in situ sensor elevation.

3 Methods: Models

To interpret hydrologic timeseries described in the previous section, we apply two classes of models that are commensurate in complexity with the data.

3.1 Falling Head Permeameter Model

For lake drainage, we recognize similarities in this process to a falling head permeameter – a laboratory test in which drainage of a saturated porous sample is used to characterize sample conductivity through changes in height of a connected water column. We can thus use the lake drainage timeseries to back out hydrogeologic properties of the lake's volcanic bedrock. In a falling head permeameter, changes in water level over time can be related to hydraulic conductivity as

$$K = -\frac{L}{\tau} \ln\left(\frac{h_f}{h_i}\right), \tag{1}$$

where K is hydraulic conductivity (units of m/s), L is length of the flow path taken in the subsurface, h_i is the initial hydraulic head (lake level), h_f is the final level, and τ is the elapsed time (Fetter, 2001). We focus on major losses of water lasting more than 14 days (Figure 4c). We take the lake level when a drainage event starts, the lake level when it stops, and the duration of the events. We account for evaporation by multiplying the drainage duration by the daily evaporation rate and adding that to the final lake level.

In contrast to laboratory falling head permeameter experiments where geometry is known, the biggest source of uncertainty in equation 1, apart from K, is the length

L. Straight lines from Fish and Lost Lakes to Clear Lake are used, 2150 m and 10,000 m respectively, but there is no way to know the exact flow paths groundwater takes between these lakes. The Sand Mountain Volcanic Field is in between Lost Lake and Clear Lake (Figure 1c). It is possible that these vent structures intercept water (Deligne et al., 2016). Given that 0.9 km^3/year of water flows across the Cascade Crest into the Metolius river watershed (Gannett et al., 2017) adjacent to Clear Lake, it's possible (although unlikely) that the groundwater divide is between Lost Lake and Clear Lake. However, Fish Lake almost certainly drains into Clear Lake as there is an ephemeral stream linking the two.

Another source of uncertainty is that equation 1 assumes a homogeneous, isotropic porous medium. In reality, the aquifer is highly anisotropic and heterogeneous (Ingebritsen et al., 1992; Saar & Manga, 2004). We expect that, following (Manga, 1996, 1997; Jefferson et al., 2006), the property we infer via this model is horizontal hydraulic conductivity. Finally, it is possible that the lakes are not the water table of the regional aquifer. If the lakes are perched features, then a more complex model would be required.

If the aquifer is homogeneous, isotropic, and fully saturated, hydraulic conductivity can be related to permeability by

$$K = \frac{k\rho g}{\mu}, \tag{2}$$

where k is permeability, ρ is density of water (1000 kg/m^3, g is acceleration due to gravity (9.8 m/s^2) and μ is viscosity of water (10^{-3} Pas). If the material is anisotropic, this relation instead reflects the dominant permeability mediating flow.

3.2 Stream Recession Analysis of the McKenzie River at Clear Lake

In contrast to the simple drainage of Lost and Fish Lakes, we require a more complex model to describe summer recession of the McKenzie River at Clear Lake.

Groundwater sustains streamflow in the absence of precipitation. The falling limb of hydrographs, stream recessions, are often modeled as a power law relating changes in discharge dQ/dt to instantaneous discharge Q

$$-\frac{dQ}{dt} = aQ^b \tag{3}$$

where a can be related to aquifer properties and b the size of the aquifer via the Boussinesq equation for unconfined porous flow over a rigid substrate (Brutsaert & Nieber, 1977).

Interpretations of a and b in the literature assume a homogeneous, isotropic, rectangular, unconfined aquifer with a horizontal, impermeable base with a fully or partially penetrating stream at one end, and a no-flow boundary at the other (Brutsaert & Nieber, 1977; Brutsaert & Lopez, 1998; Parlange et al., 2001). The exponent b is often assumed to equal 1 for long time periods (making equation 3 equivalent to a "linear reservoir", Chow et al. (1988)), 1.5 for a "late-time" solution when the aquifer has lost enough water that the no-flow boundary at the drainage divide influences discharge, and 3 for an "early-time" solution when the aquifer is saturated enough that the no-flow boundary does not influence the solution (Brutsaert & Nieber, 1977). Other b-values can result from relaxing the initial assumptions. For example, b can equal 2 for a late-time solution if permeability has a power-law relationship with depth (Rupp & Selker, 2005), and can equal 0 for shallow, sloping aquifers (Bogaart et al., 2013).

At low discharge q, change in discharge dq is often less than measurement precision of the stream gauge, leading to horizontal banding that can impact curve-fitting (Rupp & Selker, 2006). There are several different techniques to reduce this impact (Tallaksen,

1995; Rupp & Selker, 2006; Tashie et al., 2020), we choose to perform a "master recession" analysis that shows the average response of the system at high and low flow.

Recession periods are identified by finding consecutive days where the change in mean daily discharge with time ($\frac{dq}{dt}$, where $dt = 1$) is negative. If a recession period lasts longer than 3 days, we take the median discharge and mean change in discharge, reducing the event to a single point in the point cloud, and plot it on a log-log graph (Figure 8a-b). Change in discharge can be related to discharge with equation 3.

In general, a depends on the value of b (Brutsaert & Nieber, 1977). Traditionally, a $b = 1.5$ and a $b = 3$ curve is fit to the lower envelope of the recession point cloud. The inflection point where the aquifer changes from an early to a late-time solution can solve the system of equations for aquifer properties (Parlange et al., 2001). However, this approach assumes that the late-time solution is applicable for small Q, and the early-time for large Q. The opposite relationship is found in the High Cascades (Tague & Grant, 2004), so direct applicability of these equations is unclear and warrants further study (likely requiring numerical solutions that account for known layered structure (Saar & Manga, 2004; Rupp & Selker, 2005; Ingebritsen et al., 1992)).

Instead, we elect to model the long summer recession as the drainage of parallel linear reservoirs. This approach can still provide insight into the recession exponent b, because the ratio of reservoir retention times for 2 parallel linear reservoirs can be linked to the recession exponent.

3.3 Linear Reservoir Model

Given an average characterization of recession through the master recession exponent, we can now focus on the summer recession specifically. To do so we employ linear reservoir theory, a common semi-empirical framework for modeling hydrologic systems (Chow et al., 1988).

A linear reservoir is one in which discharge (Q) is linearly proportional to storage (S), $Q = \alpha S$. α is the reservoir constant. It has units of time^{-1}, its inverse is often called the reservoir retention time, the time it takes for initial storage or discharge to decay by e. In the event that $b = 1$, this is a in equation 3.

Summer recession is isolated with the same technique in the previous section, except it must last at least 100 days. We chose this cutoff for several reasons. First, is to allow for a transition from quick flow to slow flow, and a long tail end of slow flow. Second is to filter out years with a summer rainstorm that interrupted the summer recession. The longest recession event of the calendar year, as the summer recession can often last until the beginning of the new water year in October, is isolated. 31 out of 35 years had a recession event that met these criteria, always in the summer. During the tail end of summer recessions, there are often small ($\sim$ 1 cfs) oscillations in discharge with no corresponding precipitation events at the SNOTEL sites. We assume that these are instrument error and smooth the hydrograph with a savgol filter (Savitzky & Golay, 1964) (with polynomial order 3, and a window length of 15) to get rid of this effect, but we fit the model to the unsmoothed data.

We first model summer recession as the drainage of a single linear reservoir, but this does not adequately model the behavior of the system (Figure 8a). Summer recession from Clear Lake exhibits 2 slopes, quick drainage at the beginning of the recession, then slow drainage for the rest of summer (Figure 8a, Figure 4b). The two slopes are well fit with 2 parallel linear reservoirs (Rimmer & Hartmann, 2012; Bonacci, 1993) with reservoir constants α_s and α_f. The ratio of reservoir constants r_α can be related to recession b-value via

$$r_a = \frac{\alpha_f}{\alpha_s} = \frac{4b - 2 \pm \sqrt{(2-4b)^2 - 4}}{2}, \tag{4}$$

(Gao et al., 2017; Roques et al., 2022).

The summer hydrograph from Clear Lake is the sum of discharge from both of these reservoirs,

$$Q = nQ_0e^{-\alpha_s t} + (1-n)Q_0e^{-\alpha_f t}, \tag{5}$$

where Q_0 is the initial discharge, n is the fraction of Q_0 arising from the slow flow reservoir, and $\alpha_f = \alpha_s/r_\alpha$.

In a similar manner to the falling head permeameter model, we can relate these reservoir constants to hydraulic properties. Provided that a linear reservoir is well approximated by a Boussinesq aquifer (Gelhar & Wilson, 1974), reservoir constant α_i (with $i = s, f$) can be related to aquifer properties with

$$\alpha_i = \frac{3T_i}{\phi_i L_i^2}, \tag{6}$$

where T_i is transmissivity (m^2/s) for each reservoir, ϕ_i is porosity, and L_i is aquifer length (Gelhar & Wilson, 1974). Because there is no assumed spatial relationship between the parallel fast and slow reservoirs, in general these parameters can be distinct.

4 Results

Our integration of direct and remote sensing of summer lake drainage with analysis of the Clear Lake hydrograph allows us to understand surface water dynamics in the absence of significant precipitation influence simultaneously at multiple scales within a volcanic drainage basin. We discuss our results in the following order: lake drainage, falling head permeameter model, stream recession analysis of the McKenzie River at the outlet of Clear Lake, and linear reservoir modeling.

4.1 Lake Draining

Lost and Fish Lakes only fill from snowmelt, as seen in Figure 4c. Summer rainfall in 2023 had negligible impact on lake levels. Both lakes drain completely over the course of 1-2 months in the summer, at an average rate of 4 cm/day for Lost Lake, 11 cm/day for Fish Lake. Both rates outpace the assumed evaporation rate of 2 mm/day, meaning that water loss is primarily into the ground. There are also smaller filling and draining events during the winter, associated with water accumulation from specific storms. A lack of wells in the study area, and inferred residence times of 7 years (Jefferson et al., 2006) make constraining flowpaths with any certainty challenging. Lost Lake and Fish Lake are small relative to Clear Lake's discharge. Their combined volumes (when full) are 33% of Clear Lake's volume, but only account for $\sim 4\%$ of Clear Lake's summer discharge. Therefore, their drainage constitutes only a minor perturbation to Clear Lake's hydrograph. All three lakes had similar average temperatures of $\sim 5°C$ from December 2023 - June 2024, a period when all lakes were filled with water.

While the rates are similar for all years measured, the timing of lake drainage has not been constant. Over 30 years from 1990-2021, Lost Lake drainage time has shifted systematically earlier in the summer, from October to July (Figure 10a). This shift corresponds to declining maximum snowpack depths in the region (Figure 10b, f). Lost lake also fills earlier in the year, as snow melts earlier with warming temperatures, but it reaches the same maximum volume. Fish Lake consistently drains by August over our 30 year dataset (Figure 10c), but fills earlier in the year and reaches a larger maximum volume. Fish Lake's behavior could reflect a faster snowmelt, or increasing winter rainfall.

In contrast to Lost and Fish Lake, Clear Lake's surface area is nearly static seasonally over our 30 year GSWO dataset. It discharges 27 times its volume from its outlet each water year on average, and 8 times its volume during summer recession on average. Thus, flow during summer recessions must be entirely groundwater flow from the

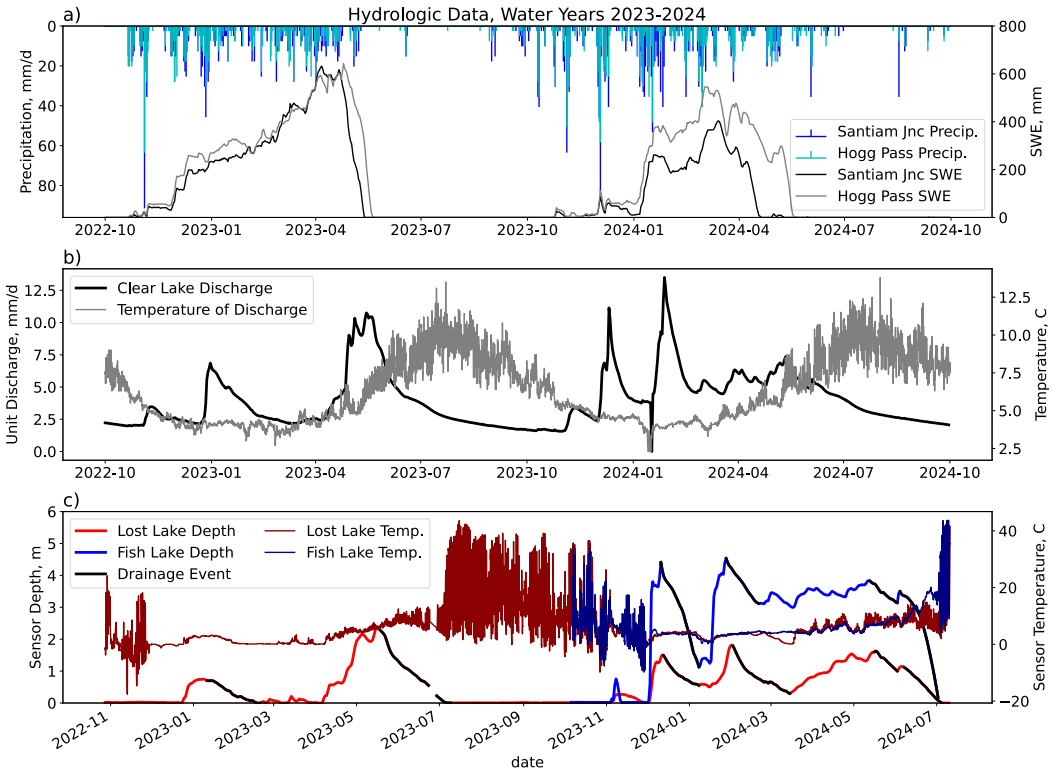

Figure 4. Hydrologic data for the 2023-2024 water years. Note different X axes between panels. a) Precipitation and Snow Water Equivalent (SWE) from Santiam Jnc and Hogg Pass SNOTEL stations. b) Clear Lake daily mean discharge and hourly water temperature, from USGS-14158500. c) Lost and Fish Lake mean daily sensor depths and hourly water temperatures, collected as part of this study. Lake drainage events used in modeling highlighted in black. The data gap for Lost Lake in 2023 was a result of the sensor being temporarily removed, drainage from May 2023 to July 2023 is treated as a single event.

aquifer to sustain streamflow and lake levels. Clear Lake is also seeing declining summer streamflow with declining snowpack (Figure 10e), by 9% percent over 30 years.

4.2 Falling Head Permeameter Model

We identified 6 drainage events for Lost Lake and 4 for Fish Lake for the 2023-2024 water years from the in situ sensors. Remote sensing data only captured the summer drainage. 0.77×10^6 m^3 drains out of Lost Lake in 44 days on average, 2.2×10^6 m^3 out of Fish Lake in 44 days. The log-ratio of final to initial lake level is plotted against elapsed time in equation 1 and hydraulic conductivity K is calculated from the slope (Figure 7). Permeability is calculated from equation 2, and reported as an order of magnitude due to the many simplifying assumptions made in this model. Permeability of Lost Lake is on the order of 10^{-10} m^2, while Fish Lake is smaller, 10^{-11} m^2. Uncertainty from the 95% confidence intervals does not change the order of magnitude of permeability for either lake. Permeability in the region is both anisotropic and decreases with depth (Ingebritsen et al., 1992; Saar & Manga, 2004). These values are within the range of near-surface horizontal permeabilities from previous studies, 10^{-11} m^2-10^{-9} m^2 (Manga, 1997; Jefferson et al., 2006), but outside the range of bulk horizontal permeabilities incorporating deeper flow, 10^{-14} m^2-10^{-12} m^2 (Ingebritsen et al., 1992; Saar & Manga, 2004), and larger

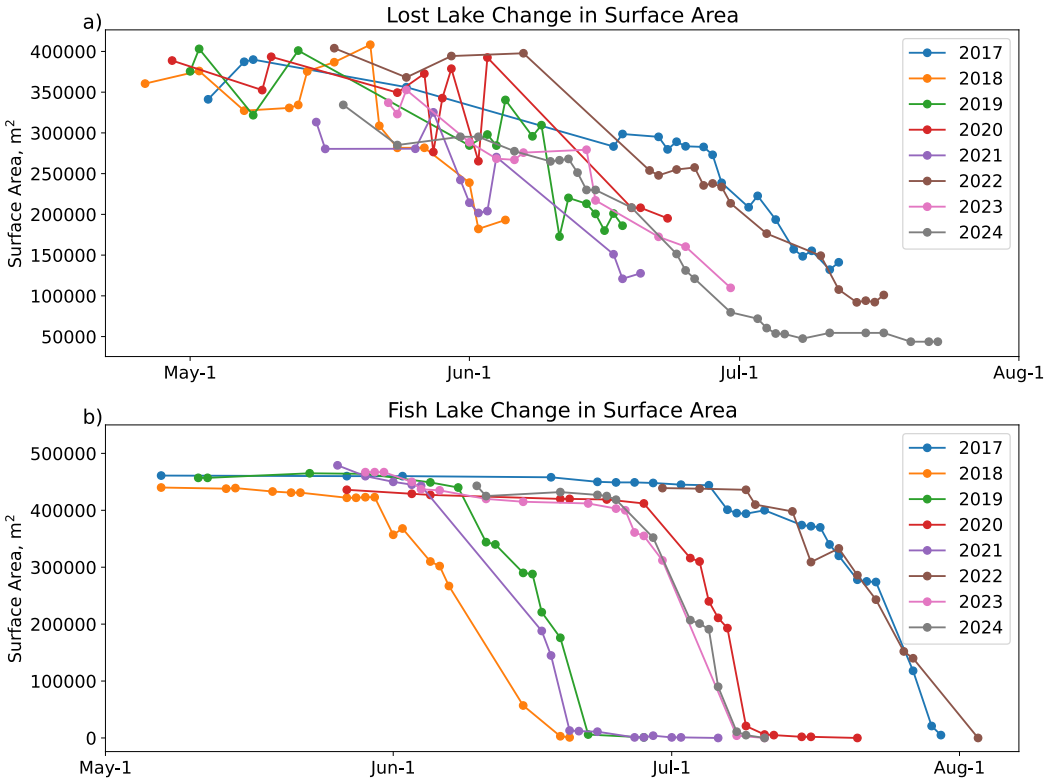

Figure 5. Lost (a) and Fish (b) Lake surface area time series from Planet data.

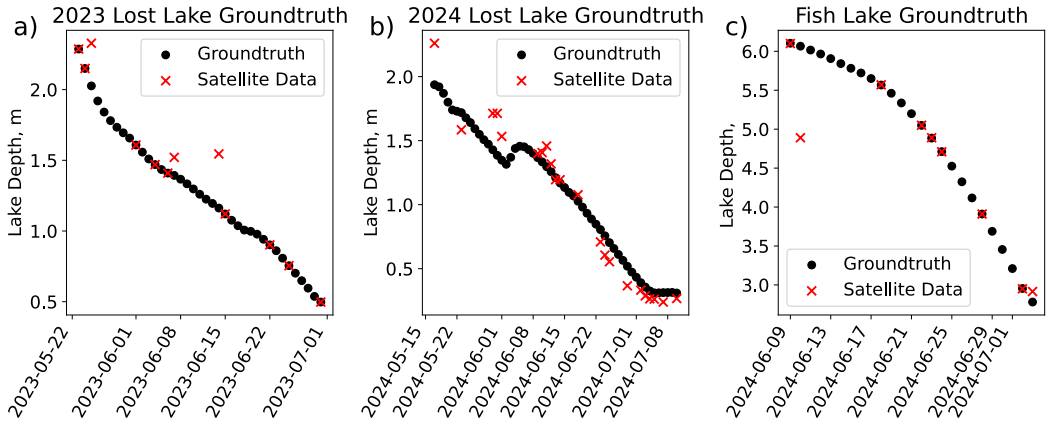

Figure 6. Sentinel-2 derived lake depths compared to measured lake depths for Lost Lake in 2023 (a) and 2024 (b), and Fish Lake in 2024 (c).

than vertical permeability, 10^{-14} m^2 (Saar & Manga, 2004). For comparison, "permeable basalt" can range from 10^{-15} m^2-10^{-10} m^2, "clean sand" from 10^{-9} m^2-10^{-5} m^2, and gravel from 10^{-6} m^2-10^{-3} m^2 (Freeze & Cherry, 1979).

4.3 Stream Recession Analysis and Linear Reservoir Modeling

Fitting equation 3 to the point cloud of streamflow recession events yields $b = 2.07 \pm 0.07$ (95% CI). The physical meaning of this value is discussed later. From equation 4,

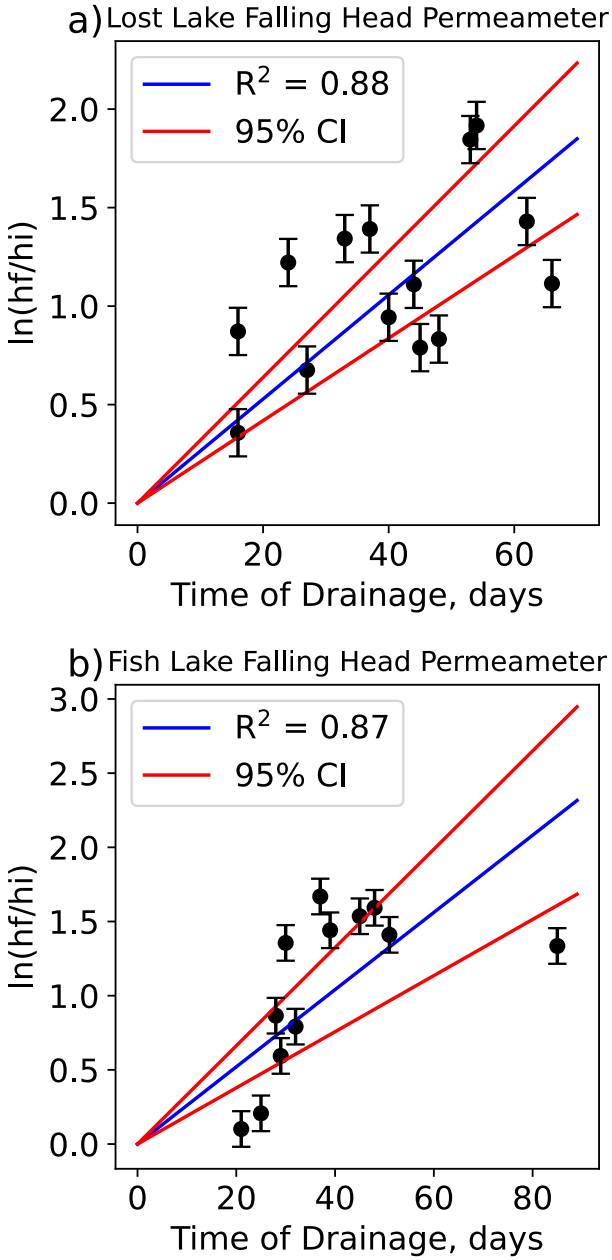

Figure 7. Graph of log lake drainage vs. time until drained, where h_f is the final height of water above sensor and h_i is the initial height of water, based on equation 1, for **(a)** Lost **(b)** and Fish lakes. The slope of the line and 95% Confidence Intervals (CI) is related to hydraulic conductivity through equation 1

this means that slow reservoir retention time is roughly 6 times longer than quick reservoir retention time. The slow reservoir has a mean retention time of 165 ± 40 days, and the quick reservoir's is 27 ± 7 days (Figure 8b). There is a correlation between reservoir constants and max Snow Water Equivalent (SWE) over 35 years (Figure 8c).

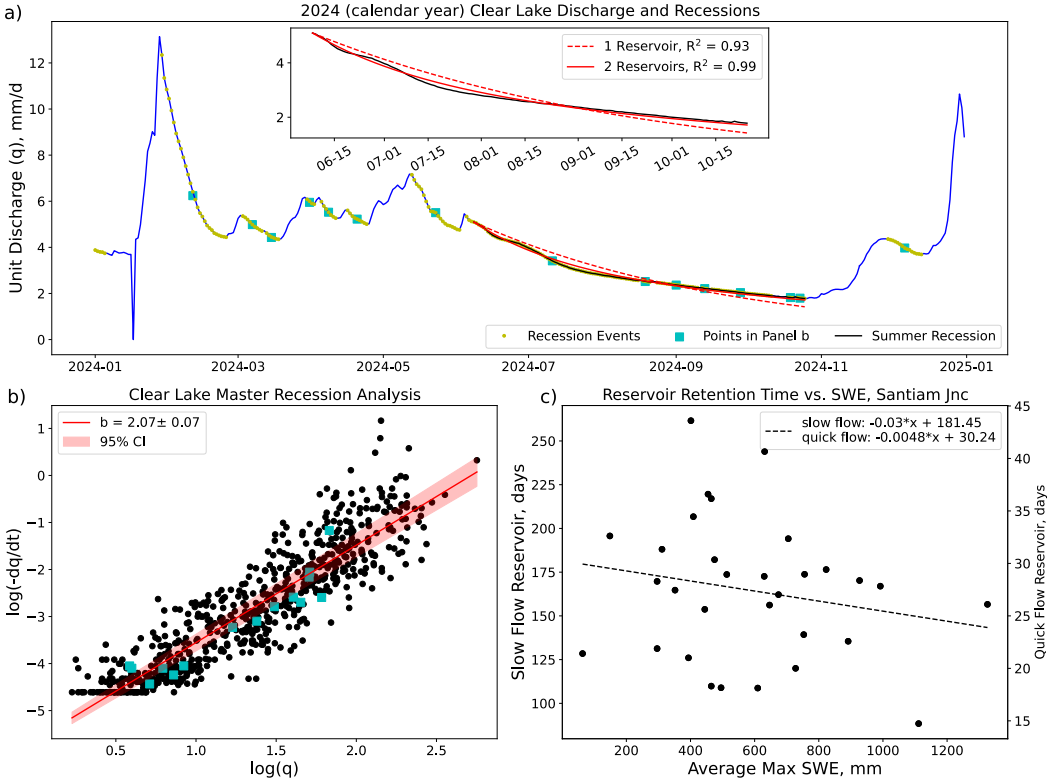

Figure 8. **(a)** Clear Lake discharge for the 2024 calendar year is used to illustrate our modeling technique for equations 3 and 4. Calendar year is used instead of water year since late summer discharge often lasts after the start of the water year. Recession events are noted as yellow dots, except for the summer recession, which is a black line. The median discharge of the entire event, which equation 3 if fit to, is noted as a blue square. The subpanel shows the summer recession fit with a linear reservoir model and two parallel linear reservoirs in more detail. **(b)** Recession plot (instantaneous discharge Q against its time rate of change dQ/dt) for recession events satisfying conditions described in the text. Red curve is least squares fit, corresponding to the recession exponent b in equation 3. 95% confidence interval (CI) is shown. The recession events from the 2024 calendar year are noted with blue squares. **(c)** Slow and fast reservoir retention times from equation 6, the inverse of the reservoir constants $(1/\alpha_s, 1/\alpha_f)$ versus max SWE at each SNOTEL station, for time spanning 1990-2024. Linear fits are dashed lines.

5 Discussion

The three lakes studied here represent streams that were dammed by Holocene lava flows from the Sand Mountain Volcanic Complex. These lava dams impede the flow of water, and lakes form as a result, with lake size dictated by maximum recharge from snowpack and lava dam height relative to surrounding topography. The smaller Lost Lake and Fish Lake systems run out of water in the summer, the larger Clear Lake system has enough recharge to sustain streamflow and lake levels. The drainage of Lost and Fish Lakes can be explained simply by porous drainage (Darcy's Law, as embodied by equation 1). The implied permeability of the Sand Mountain lavas varies by at least an order of magnitude across its extent, which is reasonable considering the heterogeneous physical volcanology on display (Deligne et al., 2016). This range is also consistent with similar estimates of lava flow hydrogeologic properties in other locations (Lindholm, 1996;

Izuka & Rotzoll, 2023; Rotzoll & El-Kadi, 2008). In this section, we discuss several implications of our findings for the hydrogeology of young volcanic landscapes.

5.1 Hydrogeologic Structure

The three lakes studied here represent three different scales with similar origin and a similar location to assess hydrogeologic structure. Saar and Manga (2004) modeled the isothermal temperature-depth profile of a geothermal borehole at Santiam Pass, just East of (and drilled at slightly higher elevation than) Lost Lake. They found a near surface horizontal permeability of $\sim 10^{-12}$ m^2 and a vertical permeability of $\sim 10^{-14}$ m^2. Ingebritsen et al. (1992) found a bulk permeability on the order of 10^{-14} for rocks > 2.3 Ma by analyzing similar borehole temperature profiles in the Oregon Cascades. Jefferson et al. (2006) studied springs flowing through the shallow crust (30 - 120 m), and found a horizontal permeability ranging from $10^{-11} - 10^{-9}$ m^2. Saar and Manga (2004), largely summarizing work from Manga (1997), also lists shallow (< 100 m), horizontal permeabilities of springs on the east slope of the High Cascades within the same range. The permeabilities implied by the drainage of Lost Lake and Fish Lake are in the range of values for the shallow crust, implying shallow, predominantly horizontal flow into the groundwater system. As depth of flow increases, permeability decreases.

The variation in reservoir constants α_s and α_f (Figure 8c) demonstrate the nonlinearity of the system (Wittenberg, 1999; Kirchner, 2009). We calculate bulk horizontal transmissivities for the two linear reservoirs that characterize drainage from Clear Lake using equation 6. The lengthscale of these compartments is uncertain, and groundwater divides may not follow topographic divides in this region. Our calculation of aquifer properties depends on the lengthscales we choose (Figure 9a). We pick geographic lengthscales, and a common porosity of 0.1 for both (Ingebritsen et al., 1992), and find transmissivities of 0.59 ± 0.15 (std.) m^2/s for the slow flow reservoir and 0.37 ± 0.1 (std.) m^2/s for the quick flow reservoir.

Previous research in the region conceptualized the High Cascades as having two compartments: shallow, quick-draining local hillslopes and a large, deep, regional aquifer sustaining summer streamflow (Tague & Grant, 2004). From this characterization, we relate the slow flow reservoir to summer drainage of the regional aquifer and the quickflow reservoir to fast-draining shallow flow paths. The quickflow reservoir could be a compartment associated with Holocene lavas or vent structures of the Sand Mountain Volcanic Field. This volcanic complex borders Clear Lake on its eastern shore, and created the lake when its lavas dammed the ancestral McKenzie River 2.9-3 ka (Stearns, 1929; Deligne, 2012). The lake levels of Lost and Fish Lakes mirror the discharge of Clear Lake (Figure 4b-c), and the seasonal lakes finish draining near the inflection point where the quickflow reservoir for Clear Lake is extinguished (Figure 4). In this scenario, Lost Lake and Fish Lake may represent the water table of this aquifer compartment.

Transmissivity is the product of aquifer thickness and hydraulic conductivity. We use the depth of isothermal or inverted temperature-depth profiles from a geothermal borehole between Clear Lake and Fish Lake (Youngquist, 1980) as a proxy for aquifer thickness, and relate hydraulic conductivity to permeability with equation 2. The isothermal section extends to a depth of 558 m (1835 ft). This would be a lower bound of aquifer thickness. We do not know how deep the isothermal section extends, drilling stopped because the drillers were only contracted for 2000 ft wells. The drill logs note a 25 m thick basalt unit at the surface. If we assume this shallow 25 m thick basalt unit is the quick flow reservoir, that implies a permeability on the order of 10^{-9} m^2, uncertainty in transmissivity did not change order of magnitude. Taking the remaining depth as the slow flow reservoir, this implies a permeability on the order of $10^{-11} - 10^{-10}$ m^2.

The quickflow reservoir may instead represent the drainage of the Western Cascade portion of Clear Lake's watershed. 25% of Clear Lake's watershed is in the Western Cas-

cade province (Figure 1b), and there are several small Western Cascades streams that flow into Clear Lake. However, much of this Western Cascades drainage is intercepted by High Cascades lava flows before it can reach Clear Lake, as in the case of the creek feeding Fish Lake. A regional study of High vs. Western Cascade stream summer recession would be needed to test between these hypotheses, to see how much variance there is within these provinces and between them through time.

We use elevation difference between the seasonal lakes and Clear Lake as proxy for aquifer thickness to calculate transmissivities of Lost Lake and Fish Lake. Figure 9b shows how the transmissivities of our study area compare regionally. Jefferson et al. (2006) looked at springs on the Western slope of the High Cascades, and used a porosity of 0.15. Manga (1997) looked at streams on the Eastern slope, and used a porosity (that he equated to specific yield) of 0.2. We see that transmissivity/specific yield has a near-linear relationship with scale length, increasing by 0.46 m^2/s per km of observation scale, indicating a highly heterogeneous aquifer (Sánchez-Vila et al., 1996). This interpretation is also supported by krigging analysis of ground-water affected lengths of geothermal borehole temperature-depth profiles. Karlstrom et al. (2025) shows that aquifer thickness is not uniform regionally. There are zones of thick aquifers, which also supports the compartmentalization of the High Cascades aquifer. Our study site is in the thickest portion of the aquifer inferred by Karlstrom et al. (2025). This thickness may be influenced by the diamict unit underlying Clear Lake, as low permeability units (such as sediments) can create thick lenses of groundwater in basalt aquifers (Izuka & Gingerich, 2003).

5.2 Insights into the hydrogeology of volcanic terrains

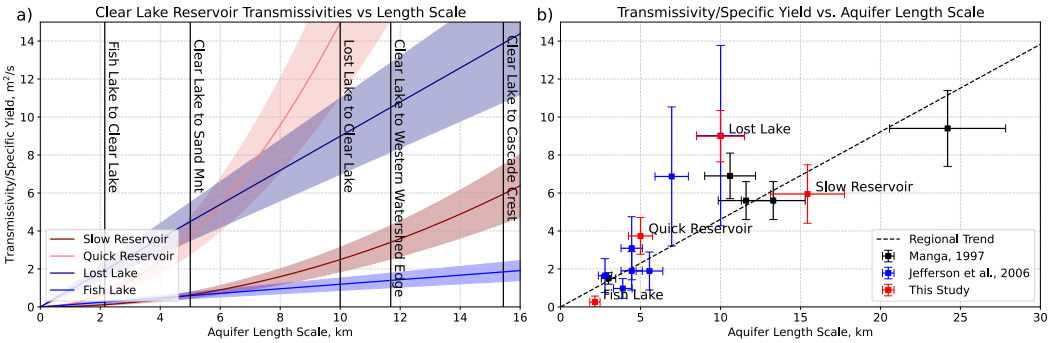

Figure 9. **(a)** Parameter trade-offs in model equations from equations 1 and 6 when applied to our study site. Graph plots Transmissivity/Specific Yield (T/S_y) versus aquifer scale length for Clear Lake, Lost Lake, Fish Lake. Error range is the standard deviation for the linear reservoir constants derived from Clear Lake data between 1990 and 2024 water years, and the 95% confidence interval bounds for Lost and Fish Lakes for 2017-2024 water years. Map distances between lakes and geographic features shown in black (Figure 1). **(b)** Best guess for geometry parameters collapses the trade-offs in (a) for T/S_y, and permits comparison to other published estimates (Manga (1997) in black and Jefferson et al. (2006) in blue). Dashed black line is a linear fit to all data points, slope of 0.46 $m^2/s/km$.

The regional increase in transmissivity with aquifer size (Figure 9b) indicates the regional aquifer is highly heterogeneous (Sánchez-Vila et al., 1996). Even the spatially and temporally coterminous lava flows Fish Lake and Lost Lake drain into vary in permeability by an order of magnitude. This is in line with other young basalt regions, where hydraulic conductivity and permeability can often range across 3-4 orders of magnitude

(Rotzoll & El-Kadi, 2008; Izuka & Rotzoll, 2023; Lindholm, 1996; Lachassagne et al., 2014; Charlier et al., 2011; Schilling et al., 2023). Compartmentalization is common in young basalt aquifers, which can be highly layered and discontinuous (Lachassagne et al., 2014; Violette et al., 2014; Schilling et al., 2023; Adikari, 2015). Heterogeneity could be a reflection of these features.

The intrinsic physical properties of lava flows, and variation in hydrogeologic structure as flows age, likely control this heterogeneity. The variable age of lava flows impacts water flow both from fines infiltration (e.g., volcanic ash or glacial till from regional deposits) and chemical weathering (clay formation). The thickness of lava flows is a known factor (Izuka & Rotzoll, 2023). Much of the permeability of lava flows comes from interflow zones (rubbly flow tops and bottoms) (Manga, 2001; Izuka & Rotzoll, 2023). Basalt aquifers that are a sequence of many thin flows often have a greater horizontal permeability than sequences of a few thick flows (Izuka & Rotzoll, 2023). Of course, the existence of fractures, faults, and large porosity features such as flow tubes cannot be discounted, but these features would likely manifest as controlling transmissivity at scales similar to flow length. The cluster of points on < 10 km scales similar to flows observed regionally (e.g., Figure 1b) may indicate that individual flow units have transmissivity/specific yield of $\sim 1-2$ m^2/s. Future research is needed to quantify how these factors control permeability.

Lava flows damming rivers are a characteristic feature of volcanic landscape evolution, and the apparent stability of these features in our study area represent a contrast to lava dams in other systems. The longevity of lava dams (and associated lakes) vary between ≤ 1 year for historical eruptions such as Laki in Iceland (Boreham et al., 2020), 1-100's years in the Colorado River (Crow et al., 2015), to potentially $\sim 1-10$ ka in the Deschutes (Deligne et al., 2017) and Owyhee River (Ely et al., 2012). Permeability of emplaced lavas, such as we infer here, as well as hydrologic properties of the substrate, river discharge, and pre-existing topography, all seem to be factors for lava dam longevity (Boreham et al., 2020).

We end this section by noting that the ephemeral hydrologic features we have focused on in the Central Oregon Cascades are relatively common in volcanic landscapes generally. The large vertical permeabilities of young lava flows (Ingebritsen et al., 1992; Saar & Manga, 2004; Karlstrom et al., 2025) results in low surface runoff (Urrutia et al., 2019; Tague & Grant, 2004; Karlstrom et al., 2025; Manga, 1997) and losing streams (Lachassagne et al., 2014; Charlier et al., 2011). Many aquifers are perched, and vertically recharge lower elevation aquifers (Violette et al., 2014; Lachassagne et al., 2014). In the Southern Washington Cascades, similar seasonally draining lakes are found in other areas where Quaternary volcanic output is dominated by mafic lava flows, such as South Prairie Lake (Hudec et al., 2019).

5.3 Resilience to Climate Change

Current projections indicate precipitation in the Oregon Cascade Range will switch from snow dominated to rain dominated due to projected air temperature increases over the next 50 years (Fleishman, 2025). Total precipitation is expected to remain static or increase by a small amount, while snowpack is predicted to decrease by 45% in the Cascade Range by mid-century (2045-2074) (Fleishman, 2025). This new regime may cause higher winter streamflow, but lower summer streamflow (Tague et al., 2008). Western Cascade streams are predicted to see a larger percent-reduction in summer streamflow, and High Cascade streams are predicted to see a larger absolute reduction (Tague et al., 2008). The long term changes in lake drainage patterns between Lost Lake and Fish Lake reflect these predictions. Fish Lake was a Western Cascade stream before being dammed, Lost Lake was a High Cascade stream. Both draining lakes have been impacted by de-

creasing snowpack, but Lost Lake dramatically so (Figure 10). Over the past 30 years, Lost Lake went from having water into October to being dry by July.

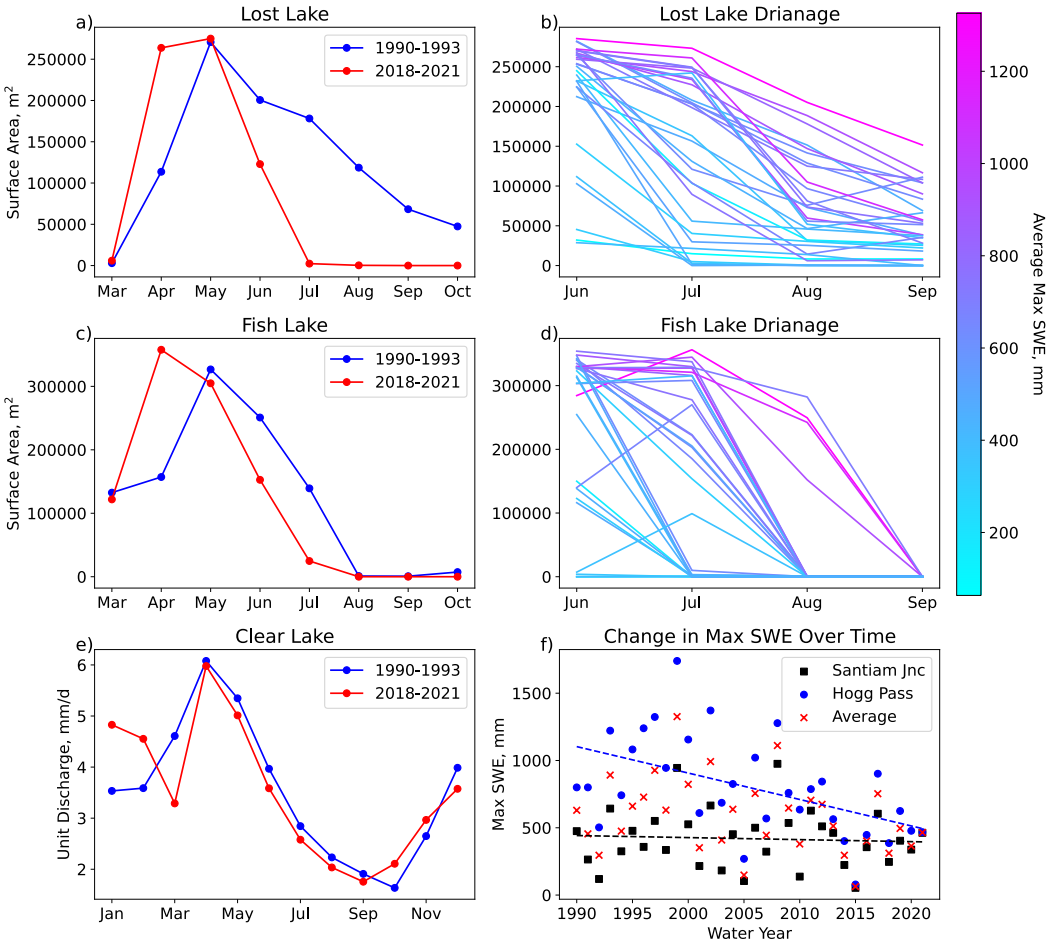

Figure 10. a and c) Average monthly lake surface areas for first and last 5 years of available ESA GSWO data for Lost (a) and Fish (c) lakes. b and d) Lost (b) and Fish (d) Lake drainage curves for every year, colored by max SWE. Lakes are draining earlier in the year as snowpacks decrease. e) Average monthly discharge from the outlet of Clear Lake. f) Max SWE each water year over time. Hogg Pass is losing 19 mm/year on average, Santiam Junction 0.4 mm/year. Decrease in surface area and discharge over 30 years is observed, correlating with a decrease in SWE.

Western Cascade streams are fed by local hillslope aquifers and experience a prolonged summer recession and low baseflows (Tague & Grant, 2004). The system that fed Fish Lake always ran out of water in the summer as a result. High Cascade streams are fed by both their local hillslopes and a large, regional aquifer which sustains high summer baseflows (Tague & Grant, 2004) and may not follow topographic boundaries (James et al., 2000; Jefferson et al., 2006; Gannett et al., 2017). The system that feeds Lost Lake used to sustain it well into October, at least. Now, we infer that the High Cascade Lost Lake is behaving more like the Western Cascade Fish Lake and is now primarily recharged by its local hillslopes.

A change this dramatic has not propagated downstream to Clear Lake. The decline in snowpack that caused a total decline in summer lake levels for Lost Lake have only caused a 9% decline in mean-daily August streamflow out of Clear Lake (Figure 10e), and our recession analysis shows that Clear Lake is still in an "early time" regime. Lost Lake is at a higher elevation than Clear Lake, this could mean the water table has fallen below Lost Lake but is still sustaining Clear Lake. Geothermal boreholes in the region support this interpretation. Isothermal or inverted temperature-depth profiles imply aquifer thicknesses of around 600 m near Clear Lake, and 1000 m at Santiam Pass. These are almost certainly lower bounds on aquifer thickness, the drilling ceased before an end to these profiles was reached due to contracting. However, more work is needed to quantify the impact projected decreases in snowpack will have on Clear Lake, the High Cascades Regional Aquifer, or other groundwater-fed lakes in the High Cascades, such as Waldo Lake or Big Lake (Johnson et al., 1985).

6 Conclusion

The highly permeable basaltic bedrock that constructs the Oregon Cascades, combined with the high precipitation, creates a large groundwater system. Regionally, this groundwater system is heterogeneous and compartmentalized, which is reflected in a near-linear relation between transmissivity/specific yield and lengthscale of slope 0.46 $m^2/s/km$. This young volcanic landscape hydrologically behaves less like a fractured mountain landscape and more like an immature karst landscape (Ford & Williams, 2007) due to lava flow structures like cooling joints, breccia, and lava tubes. The lava flows that constructed this landscape buried existing terrain, damming streams that form lakes when inundated by water in the spring snow melt. The time it takes these lakes to drain is controlled by the permeability of these basalt dams. As snowpacks decrease, these lakes drain sooner. Fish Lake, a dammed Western Cascade stream, has not seen a dramatic change. Lost Lake, a dammed High Cascade stream, has changed dramatically. Over 30 years, drainage time has shift from October to July (Figure 10a). Impacts of declining snowpack are also observed in the larger Clear Lake system, although it appears more resilient than the smaller subsystems of Fish and Lost Lake. Our results highlight how volcanic history controls the movement of water in mafic landscapes.

7 Open Research

Pressure-temperature and surface area data from Lost and Fish Lakes have been deposited on hydroshare `http://www.hydroshare.org/resource/3f5bc470cd924b9494dbb429777c4a56`. Clear Lake discharge and temperature data was downloaded from `https://waterdata.usgs.gov/nwis`. SNOTEL data was downloaded from `https://wcc.sc.egov.usda.gov/nwcc/tabget`. ESA GWSO data was downloaded from `https://global-surface-water.appspot.com/download`.

Acknowledgments
We would like to acknowledge fruitful discussions with Gordon Grant, Kathy Cashman, and Becky Fasthe about central Oregon Cascades hydrology and volcanic structure during the preparation of this manuscript. Measurements at Lost and Fish Lake were carried out with permission of the Willamette National Forest Mckenzie River Ranger District.

Appendix A Converting Pressure-Transducer Data into Water Depth

We measure lake water depth variations in the following way. In August, when Lost Lake and Fish Lake are drained, Onset Hobo Pressure-Temperature transducers are strapped to rebar using zip ties, then driven into the lakebed so that the sensor is as close to the

lakebed as possible (a few centimeters above it). These sensors are also strapped to trees (above snow depth) outside the shoreline to correct for atmospheric pressure fluctuations (Figure 2). Water pressure (maximum error 0.62 kPa, Onset (n.d.)) is converted to height of water above each lakebed sensor via hydrostatic balance $P = \rho g h$, where P is pressure, ρ is density of water, g is acceleration due to gravity, and h is depth of water over the sensor.

Water temperature (accuracy ±0.44°C, Onset (n.d.)) is also collected by the pressure transducers, and is used in winter to confirm that the pressure change is from water and not snow. When covered with water, there is little diurnal variation in the temperature time series compared to when the sensor is in the air (Figure 4c).

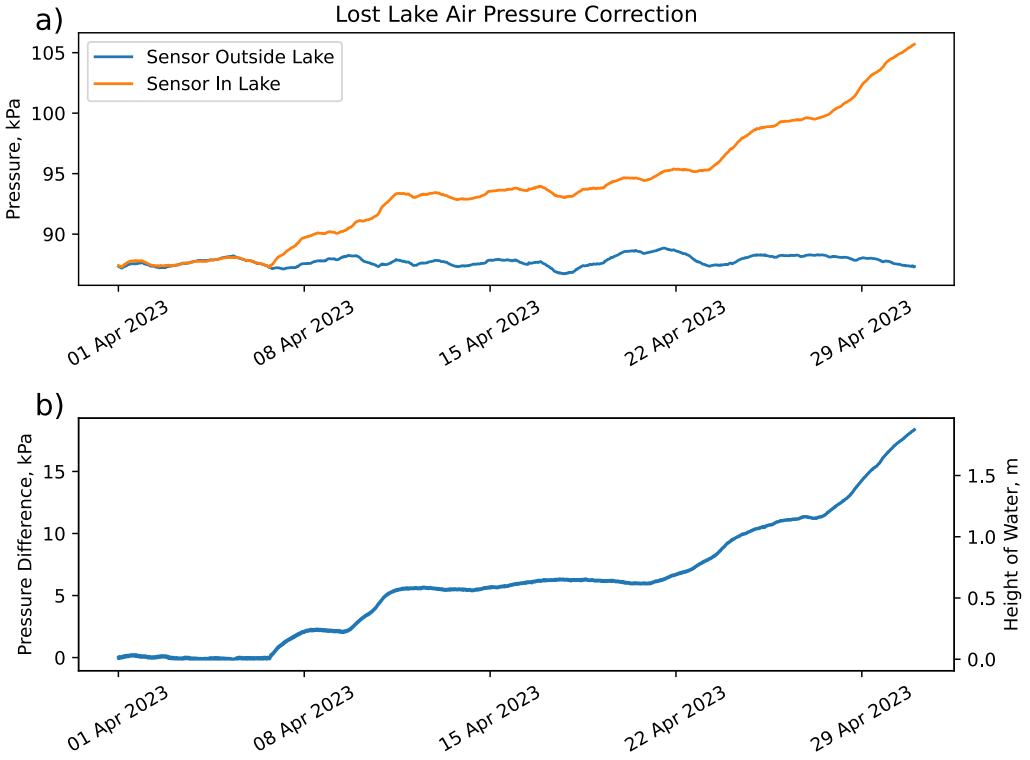

Figure A1. Pressure correction for the lake sensors. a) Pressure on the lakebed compared to air pressure. b) Water pressure on the lakebed after correcting for atmospheric pressure.

References

Adikari, D. P. (2015). Hydrogeological features of Mount Fuji and the surrounding area, Central Japan: An overview. *Journal of Institute of Science and Technology*, *19*(1), 96–105. doi: https://doi.org/10.3126/jist.v19i1.13834

Black, G. L., Woller, N. M., & Ferns, M. L. (1987). *Geologic map of the Crescent Mountain area, Linn County, Oregon.* GMS-47. Portland, OR: DOGAMI.

Bogaart, P. W., Rupp, D. E., Selker, J. S., & van der Velde, Y. (2013). Late-time drainage from a sloping boussinesq aquifer. *Water Resources Research*, *49*(11), 7498-7507. doi: https://doi.org/10.1002/2013WR013780

Bonacci, O. (1993). Karst springs hydrographs as indicators of karst aquifers. *Hydrological Sciences Journal*, *38*(1), 51-62. doi: https://doi.org/10.1080/

02626669309492639

Boreham, F., Cashman, K., & Rust, A. (2020). Hazards from lava–river interactions during the 1783–1784 Laki fissure eruption. *GSA Bulletin*, *132*(11-12), 2651-2668. doi: https://doi.org/10.1130/B35183.1

Brooks, J. R., Johnson, H. M., Johnson, K., Cline, S. P., Comeleo, R., Rugh, W., & Trine, L. (2025). Inferring snowpack contributions and the mean elevation of source water to streamflow in the Willamette River, Oregon using water stable isotopes. *Hydrological Processes*, *39*(5), e70136. doi: https://doi.org/10.1002/hyp.70136

Brutsaert, W., & Lopez, J. P. (1998). Basin-scale geohydrologic drought flow features of riparian aquifers in the Southern Great Plains. *Water Resources Research*, *34*(2), 233-240. doi: https://doi.org/10.1029/97WR03068

Brutsaert, W., & Nieber, J. L. (1977). Regionalized drought flow hydrographs from a mature glaciated plateau. *Water Resources Research*, *13*(3), 637-643. doi: https://doi.org/10.1029/WR013i003p00637

Charlier, J.-B., Lachassagne, P., Ladouche, B., Cattan, P., Moussa, R., & Voltz, M. (2011). Structure and hydrogeological functioning of an insular tropical humid andesitic volcanic watershed: A multi-disciplinary experimental approach. *Journal of Hydrology*, *398*(3), 155-170. doi: https://doi.org/10.1016/j.jhydrol.2010.10.006

Chow, V., Maidment, D., & Mays, L. (1988). *Applied hydrology.* New York, NY: McGraw-Hill.

Crow, R. S., Karlstrom, K. E., McIntosh, W., Peters, L., Crossey, L., & Eyster, A. (2015). A new model for Quaternary lava dams in Grand Canyon based on 40Ar/39Ar dating, basalt geochemistry, and field mapping. *Geosphere*, *11*(5), 1305-1342. doi: https://doi.org/10.1130/GES01128.1

Deligne, N. I. (2012). *After the flow: landscape response to the emplacement of Holocene lava flows, Central Oregon Cascades, USA* (Unpublished doctoral dissertation). University of Oregon, Eugene, OR.

Deligne, N. I., Conrey, R. M., Cashman, K. V., Champion, D. E., & Amidon, W. H. (2016). Holocene volcanism of the upper McKenzie River catchment, central Oregon Cascades, USA. *GSA Bulletin*, *128*(11-12), 1618-1635. doi: https://doi.org/10.1130/B31405.1

Deligne, N. I., Mckay, D., Conrey, R., Grant, G. E., Johnson, E. R., O'Connor, J., & Sweeney, K. (2017). *Field-trip guide to mafic volcanism of the Cascade Range in Central Oregon—a volcanic, tectonic, hydrologic, and geomorphic journey* (Tech. Rep.). Reston, VA: Survey, U.S. Geological. doi: https://doi.org/10.3133/sir20175022H

Ely, L. L., Brossy, C. C., House, P. K., Safran, E. B., O'Connor, J. E., Champion, D. E., ... Turrin, B. D. (2012). Owyhee River intracanyon lava flows: Does the river give a dam? *GSA Bulletin*, *124*(11-12), 1667-1687. doi: https://doi.org/10.1130/B30574.1

Fetter, C. W. (2001). *Applied hydrogeology* (4th ed ed.). Upper Saddle River, NJ: Prentice Hall.

Fleishman, E. (2025). *Seventh Oregon climate assessment* (Technical Report No. 14). Corvallis, Oregon: Oregon Climate Change Research Institute, Oregon State University. doi: https://doi.org/10.5399/osu/1181

Ford, D., & Williams, P. (2007). *Karst hydrogeology and geomorphology.* Hoboken, NJ: John Wiley Sons, Ltd. doi: https://doi.org/10.1002/9781118684986

Freeze, R., & Cherry, J. (1979). *Groundwater.* Upper Saddle River, NJ: Prentice-Hall.

Gabrielli, C., McDonnell, J., & Jarvis, W. (2012). The role of bedrock groundwater in rainfall–runoff response at hillslope and catchment scales. *Journal of Hydrology*, *450-451*, 117-133. doi: https://doi.org/10.1016/j.jhydrol.2012.05.023

Gannett, M. W., Lite, K. E., Jr, Risley, J. C., Pischel, E. M., & La Marche, J. L.

(2017). *Simulation of groundwater and surface-water flow in the upper Deschutes Basin, Oregon.* US Geological Survey. doi: https://doi.org/10.3133/sir20175097

Gao, M., Chen, X., Liu, J., Zhang, Z., & bo Cheng, Q. (2017). Using two parallel linear reservoirs to express multiple relations of power-law recession curves. *Journal of Hydrologic Engineering*, *22*(7), 04017013. doi: https://doi.org/10.1061/(ASCE)HE.1943-5584.0001518

Gelhar, L. W., & Wilson, J. L. (1974). Ground-water quality modeling. *Groundwater*, *12*(6), 399-408. doi: https://doi.org/10.1111/j.1745-6584.1974.tb03050.x

Houborg, R., & McCabe, M. F. (2016). High-resolution NDVI from Planet's constellation of Earth observing nano-satellites: A new data source for precision agriculture. *Remote Sensing*, *8*(9). doi: https://doi.org/10.3390/rs8090768

Hudec, J. L., Halofsky, J. E., Peterson, D. L., & Ho, J. J. (2019). *Climate change vulnerability and adaptation in southwest Washington.* U.S. Department of Agriculture, Forest Service, Pacific Northwest Research Station. doi: http://dx.doi.org/10.2737/PNW-GTR-977

Ingebritsen, S. E., Sherrod, D. R., & Mariner, R. H. (1992). Rates and patterns of groundwater flow in the Cascade Range Volcanic Arc, and the effect on subsurface temperatures. *Journal of Geophysical Research: Solid Earth*, *97*(B4), 4599-4627. doi: https://doi.org/10.1029/91JB03064

Izuka, S. K., & Gingerich, S. B. (2003). A thick lens of fresh groundwater in the southern Lihue Basin, Kauai, Hawaii, USA. *Hydrogeology Journal*, *11*(2), 240-248. doi: https://doi.org/10.1007/s10040-002-0233-5

Izuka, S. K., & Rotzoll, K. (2023). *Volcanic aquifers of Hawaii—contributions to assessing groundwater availability on Kauai, Oahu, and Maui* (Tech. Rep.). Reston, VA: U.S. Geological Survey. doi: https://doi.org/10.3133/pp1876

James, E., Manga, M., Rose, T., & Hudson, G. (2000). The use of temperature and the isotopes of O, H, C, and noble gases to determine the pattern and spatial extent of groundwater flow. *Journal of Hydrology*, *237*(1), 100-112. doi: https://doi.org/10.1016/S0022-1694(00)00303-6

Jefferson, A., Grant, G., Lewis, S., & Lancaster, S. (2010). Coevolution of hydrology and topography on a basalt landscape in the Oregon Cascade Range, USA. *Earth Surface Processes and Landforms*, *35*(7), 803-816. doi: https://doi.org/10.1002/esp.1976

Jefferson, A., Grant, G., & Rose, T. (2006). Influence of volcanic history on groundwater patterns on the west slope of the Oregon High Cascades. *Water Resources Research*, *42*(12). doi: https://doi.org/10.1029/2005WR004812

Johnson, D. M., Petersen, R. R., Lycan, D. R., Sweet, J. W., Neuhaus, M. E., & Schaedel, A. (1985). *Atlas of oregon lakes.* Corvallis, Or: Oregon State University Press.

Karlstrom, L., Klema, N., Grant, G. E., Finn, C., Sullivan, P. L., Cooley, S., ... McKay, D. (2025). State shifts in the deep critical zone drive landscape evolution in volcanic terrains. *Proceedings of the National Academy of Sciences*, *122*(3), e2415155122. doi: https://doi.org/10.1073/pnas.2415155122

Kirchner, J. W. (2009). Catchments as simple dynamical systems: Catchment characterization, rainfall-runoff modeling, and doing hydrology backward. *Water Resources Research*, *45*(2). doi: https://doi.org/10.1029/2008WR006912

Lachassagne, P., Aunay, B., Frissant, N., Guilbert, M., & Malard, A. (2014). High-resolution conceptual hydrogeological model of complex basaltic volcanic islands: a Mayotte, Comoros, case study. *Terra Nova*, *26*(4), 307-321. doi: https://doi.org/10.1111/ter.12102

Lindholm, G. (1996). *Summary of the Snake River plain regional aquifer-system analysis in Idaho and eastern Oregon* (Tech. Rep. No. 1408A). USGS. doi: https://doi.org/10.3133/pp1408A

Lohse, K. A., & Dietrich, W. E. (2005). Contrasting effects of soil development on

hydrological properties and flow paths. *Water Resources Research*, *41*(12). doi: https://doi.org/10.1029/2004WR003403

Manga, M. (1996). Hydrology of spring-dominated streams in the Oregon Cascades. *Water Resources Research*, *32*(8), 2435-2439. doi: https://doi.org/10.1029/96WR01238

Manga, M. (1997). A model for discharge in spring-dominated streams and implications for the transmissivity and recharge of quaternary volcanics in the Oregon Cascades. *Water Resources Research*, *33*(8), 1813-1822. doi: https://doi.org/10.1029/97WR01339

Manga, M. (2001). Using springs to study groundwater flow and active geologic processes. *Annual Review of Earth and Planetary Sciences*, *29*, 201-228. doi: https://doi.org/10.1146/annurev.earth.29.1.201

McFeeters, S. K. (1996). The use of the normalized difference water index (NDWI) in the delineation of open water features. *International Journal of Remote Sensing*, *17*(7), 1425-1432. doi: https://doi.org/10.1080/01431169608948714

McKay, D. (2012). *Recent mafic eruptions at Newberry Volcano and in the Central Oregon Cascades: Physical volcanology and implications for hazards* (Unpublished doctoral dissertation). University of Oregon, Eugene, OR.

Onset. (n.d.). *HOBO U20L water level logger (U20L-0x) manual.* `https://www.onsetcomp.com/sites/default/files/2024-01/17153-H%20U20L%20Manual_0.pdf`. (Accessed: 2025-08-11)

Otsu, N. (1979). A threshold selection method from gray-level histograms. *IEEE Transactions on Systems, Man, and Cybernetics*, *9*(1), 62-66. doi: https://doi.org/10.1109/TSMC.1979.4310076

O'Hara, D., & Karlstrom, L. (2023). The arc-scale spatial distribution of volcano erosion implies coupled magmatism and regional climate in the Cascades arc, United States. *Frontiers in Earth Science*, *Volume 11 - 2023*. doi: https://doi.org/10.3389/feart.2023.1150760

Parlange, J.-Y., Stagnitti, F., Heilig, A., Szilagyi, J., Parlange, M. B., Steenhuis, T. S., ... Li, L. (2001). Sudden drawdown and drainage of a horizontal aquifer. *Water Resources Research*, *37*(8), 2097-2101. doi: https://doi.org/10.1029/2000WR000189

Pekel, J. F., Cottam, A., Gorelick, N., & Belward, A. S. (2016). High-resolution mapping of global surface water and its long-term changes. *Nature*, *50*(418-422). doi: https://doi.org/10.1038/nature20584

Porder, S., Hilley, G. E., & Chadwick, O. A. (2007). Chemical weathering, mass loss, and dust inputs across a climate by time matrix in the Hawaiian Islands. *Earth and Planetary Science Letters*, *258*, 414-427. doi: https://doi.org/10.1016/j.epsl.2007.03.047.

Redmond, K. T. (2007). Evaporation and the hydrologic budget of Crater Lake, Oregon. In G. L. Larson, R. Collier, & M. W. Buktenica (Eds.), *Long-term limnological research and monitoring at Crater Lake, Oregon: A benchmark study of a deep and exceptionally clear montane caldera lake* (p. 29-46). Springer Netherlands. doi: https://doi.org/10.1007/978-1-4020-5824-0_3

Rimmer, A., & Hartmann, A. (2012). Simplified conceptual structures and analytical solutions for groundwater discharge using reservoir equations. In P. Nayak (Ed.), *Water resources management and modeling* (chap. 10). Rijeka: InteChOpen. doi: https://doi.org/10.5772/34803

Roques, C., Rupp, D. E., de Dreuzy, J.-R., Longuevergne, L., Jachens, E. R., Grant, G., ... Selker, J. S. (2022). Recession discharge from compartmentalized bedrock hillslopes. *Hydrology and Earth System Sciences*, *26*(16), 4391-4405. doi: https://doi.org/10.5194/hess-26-4391-2022

Rotzoll, K., & El-Kadi, A. I. (2008). Estimating hydraulic conductivity from specific capacity for Hawaii aquifers, USA. *Hydrogeology Journal*, *16*(5), 969-979. doi: https://doi.org/10.1007/s10040-007-0271-0

Rupp, D. E., & Selker, J. S. (2005). Drainage of a horizontal boussinesq aquifer with a power law hydraulic conductivity profile. *Water Resources Research*, *41*(11). doi: https://doi.org/10.1029/2005WR004241

Rupp, D. E., & Selker, J. S. (2006). Information, artifacts, and noise in dq/dtq recession analysis. *Advances in Water Resources*, *29*(2), 154-160. doi: https://doi.org/10.1016/j.advwatres.2005.03.019

Saar, M. O., & Manga, M. (2004). Depth dependence of permeability in the Oregon Cascades inferred from hydrogeologic, thermal, seismic, and magmatic modeling constraints. *Journal of Geophysical Research: Solid Earth*, *109*(B4). doi: https://doi.org/10.1029/2003JB002855

Savitzky, A., & Golay, M. J. E. (1964). Smoothing and differentiation of data by simplified least squares procedures. *Analytical Chemistry*, *36*(8), 1627-1639. doi: https://doi.org/10.1021/ac60214a047

Schilling, O. S., Nagaosa, K., Schilling, T. U., Brennwald, M. S., Sohrin, R., Tomonaga, Y., ... Kato, K. (2023). Revisiting Mt Fuji's groundwater origins with helium, vanadium and environmental DNA tracers. *Nature Water*, *1*(1), 60-73. doi: https://doi.org/10.1038/s44221-022-00001-4

Sherrod, D. R., & Smith, J. G. (2000). *Geologic map of upper Eocene to Holocene volcanic and related rocks of the Cascade Range, Oregon.* US Geological Survey, Washington, DC.

Stearns, H. (1929). Geology and water resources of the upper McKenzie Valley, Oregon. *USGS Water Supply Paper*, *597-D*. doi: https://doi.org/10.3133/wsp597D

Swarzenski, P., Dulai, H., Kroeger, K., Smith, C., Dimova, N., Storlazzi, C., ... Glenn, C. (2017). Observations of nearshore groundwater discharge: Kahekili Beach Park submarine springs, Maui, Hawaii. *Journal of Hydrology: Regional Studies*, *11*, 147-165. doi: https://doi.org/10.1016/j.ejrh.2015.12.056

Sánchez-Vila, X., Carrera, J., & Girardi, J. P. (1996). Scale effects in transmissivity. *Journal of Hydrology*, *183*(1), 1-22. doi: https://doi.org/10.1016/S0022-1694(96)80031-X

Tague, C., Farrell, M., Grant, G., Lewis, S., & Rey, S. (2007). Hydrogeologic controls on summer stream temperatures in the McKenzie River basin, Oregon. *Hydrological Processes*, *21*(24), 3288-3300. doi: https://doi.org/10.1002/hyp.6538

Tague, C., Grant, G., Farrell, M., Choate, J., & Jefferson, A. (2008). Deep groundwater mediates streamflow response to climate warming in the Oregon Cascades. *Climatic Change*, *86*(1), 189-210. doi: https://doi.org/10.1007/s10584-007-9294-8

Tague, C., & Grant, G. E. (2004). A geological framework for interpreting the low-flow regimes of Cascade streams, Willamette River Basin, Oregon. *Water Resources Research*, *40*(4). doi: https://doi.org/10.1029/2003WR002629

Tallaksen, L. (1995). A review of baseflow recession analysis. *Journal of Hydrology*, *165*(1), 349-370. doi: https://doi.org/10.1016/0022-1694(94)02540-R

Tashie, A., Pavelsky, T., & Band, L. E. (2020). An empirical reevaluation of streamflow recession analysis at the continental scale. *Water Resources Research*, *56*(1), e2019WR025448. doi: https://doi.org/10.1029/2019WR025448

Taylor, E. M. (1990). Volcanic history and tectonic development of the Central High Cascade Range, Oregon. *Journal of Geophysical Research: Solid Earth*, *95*(B12), 19611-19622. doi: https://doi.org/10.1029/JB095iB12p19611

Urrutia, J., Herrera, C., Custodio, E., Jódar, J., & Medina, A. (2019). Groundwater recharge and hydrodynamics of complex volcanic aquifers with a shallow saline lake: Laguna Tuyajto, Andean Cordillera of northern Chile. *Science of The Total Environment*, *697*, 134116. doi: https://doi.org/10.1016/j.scitotenv.2019.134116

Violette, S., d'Ozouville, N., Pryet, A., Deffontaines, B., Fortin, J., & Adelinet,

M. (2014). Hydrogeology of the Galápagos Archipelago. In *The Galápagos* (p. 167-183). American Geophysical Union (AGU). doi: https://doi.org/10.1002/9781118852538.ch9

Wittenberg, H. (1999). Baseflow recession and recharge as nonlinear storage processes. *Hydrological Processes*, *13*(5), 715-726. doi: https://doi.org/10.1002/(SICI)1099-1085(19990415)13:5⟨715::AID-HYP775⟩3.0.CO;2-N

Youngquist, W. (1980). *Geothermal gradient drilling, north-central Cascades of Oregon, 1979* (Tech. Rep.). Oregon State Dept. of Geology and Mineral Industries, Portland (USA).